Bilayer characteristics of a diether phosphonolipid analog of the major lung surfactant glycerophospholipid dipalmitoyl phosphatidylcholine

Victor Skita,[1,*,†] David W. Chester,[†] Carey J. Oliver,[†] Joe G. Turcotte,[§] and Robert H. Notter[**]

Department of Biochemistry* and Biomolecular Structure Analysis Center,† University of Connecticut Health Center, 263 Farmington Avenue, Farmington, CT 06030-2017; Department of Medicinal Chemistry,§ University of Rhode Island, Kingston, RI 02881; and Departments of Pediatrics, Chemical Engineering, and Environmental Medicine,** University of Rochester, Rochester, NY 14642

Abstract Thermal and lyotropic phase behavior was studied by X-ray diffraction and differential scanning calorimetry for a diether phosphonolipid analog (DEPN-8) of the major lung surfactant glycerophospholipid dipalmitoyl phosphatidylcholine (DPPC). DEPN-8 differs in an ether, rather than an ester, bond at the acyl chain-backbone linkage and a headgroup phosphonate (isosteric methylene substitution) versus phosphate constituent. Analysis of lamellar diffraction maxima demonstrated that at high relative humidity (98%) and temperatures below the liquid crystal phase transition (~45°C), DEPN-8 formed interdigitated bilayers with a characteristic periodicity of 41.9–46.5 Å. At low humidity the gel phase DEPN-8 bilayers were characteristic of a normal L_{β} phase with a periodicity equivalent to DPPC (57–59 Å). Above the liquid crystal thermal phase transition, bilayer spacing for both DEPN-8 and DPPC was 51–52 Å, characteristic of the L_{α} phase. Complete assessments of both lamellar and in-plane X-ray scattering used to construct electron density profiles and structure-factor plots for DEPN-8 defined more fully the interdigitated bilayer state at high humidity and low temperature. Compared to DPPC, it is energetically favorable for DEPN-8 to form interdigitated bilayers under conditions of excess water and low temperature. The flexible character of the ether bonds in DEPN-8 allows increased hydrophobic interactions between acyl chains, without generating a steric penalty from the increased packing density of the molecules. Additionally, the ether bond and the phosphonate moiety may allow for more energetically favorable interactions between the choline portion of the headgroup and water. The DEPN-8 ether linkage may also contribute to the improved adsorption and film respreading found previously for this phosphonolipid compared to DPPC.—**Skita, V., D. W. Chester, C. J. Oliver, J. G. Turcotte, and R. H. Notter.** Bilayer characteristics of a diether phosphonolipid analog of the major lung surfactant glycerophospholipid dipalmitoyl phosphatidylcholine. *J. Lipid Res.* 1995. **36:** 1116–1127.

Supplementary key words DEPN • interdigitated lamellar phase • X-ray diffraction • differential scanning calorimetry

The physical chemical behavior of phospholipids in hydrated bilayers underlies their biological activity as components of cell and organelle membranes. Phospholipids by their amphipilic nature are ideally suited as the building blocks of interfacial structures. They interact with water, ions, water soluble proteins and molecules, membrane proteins and receptors, and other membrane and cell components. The interactions of phospholipids in bilayers and related aggregates is also relevant for the activity of pulmonary surfactant, a complex mixture of glycerophospholipids and specific apoproteins synthesized and secreted by type II epithelial cells in the alveoli of the mammalian lung (1, 2). Such interactions affect not only the adsorption of lung surfactant to the alveolar air–hypophase interface, but also its surface tension lowering and respreading under dynamic compression in the resultant interfacial film during breathing (3, 4). Although a significant amount of research on phospholipid bilayers and the surface activity of phospholipid films has been done (see ref. 5), little information is available on bilayer characteristics that correlate with specific interfacial properties important for lung surfactant.

To help define relationships between the molecular structure and surface active behavior of phospholipid-like molecules, Turcotte et al. (6–8) have synthesized a series of eleven phosphonolipid compounds, all with saturated C_{16} acyl chain moieties similar to dipalmitoyl phosphatidylcholine (DPPC), the most prominent molecular constituent of pulmonary surfactant (3, 4). In addition to a headgroup phosphonate, these compounds have amide or ether (rather than ester) linkages at the alkyl chain-backbone junction, and a range of N-headgroups from quaternary ammonium forms through primary amines

Abbreviations: DSC, differential scanning calorimetry; MLV, multilamellar vesicles; rh, relative humidity; PSD, position-sensitive detector.

[1]To whom correspondence should be addressed.

(6–8). Studies of the dynamic surface activity of these phosphonolipids in surface films and in dispersions show that several have surface tension lowering ability equivalent to DPPC, while exhibiting more rapid adsorption and/or better film respreading during repetitive cycling (6–10). The present study investigates in detail the bilayer behavior of one such compound (DEPN-8), a diether phosphonolipid analog of dipalmitoyl phosphatidylcholine (7). X-ray diffraction and differential scanning colorimetry (DSC) are used to measure physical properties of oriented multilayer samples of DEPN-8 and DPPC as a function of temperature and hydration. The experiments demonstrate that at temperatures below its liquid crystal transition, the highly hydrated phosphonolipid analog forms interdigitated bilayers at high relative humidity. This property may contribute significantly to the improved film respreading found previously for DEPN-8 compared to DPPC (7, 9, 10).

MATERIALS AND METHODS

Phosphonolipids and phospholipids

1,2-Dipalmitoyl-*sn*-glycero-3-phosphocholine (DPPC) was purchased from Avanti Polar Lipids (Alabaster, AL) at a purity of >99%. Trimethyl (3-phosphonopropyl) ammonium (R)(S)-mono (2,3-bis-(hexadecyloxy)-propyl) ester (DEPN-8) was synthesized according to methods defined previously (8). Both DPPC and DEPN-8 gave single spots on thin-layer chromatography with solvent system C (11), and DEPN-8 was > 98% pure with a single minor contaminant on one-dimensional thin-layer chromatography with $CHCl_3$-CH_3OH-20% CH_3NH_2-H_2O 60:36:10:0.3 (v/v). DEPN-8 purity was also verified to be unchanged at the conclusion of selected calorimetry and X-ray experiments.

Sample preparation

Oriented multilayer stacks of DEPN-8 and DPPC for X-ray diffraction or DSC were prepared from sonicated dispersions of multilamellar vesicles (MLVs). Solid DEPN-8 was added to distilled water (1 mg/ml) at room temperature, sonicated briefly (<5 sec) in a bath sonicator (Bransonic 12, Branson Cleaning Equipment Co., Shelton, CT) to break up large particles, and cycled through a minimum of three freeze–thaw cycles (cooling with dry ice–acetone mixture, heating to 45–48°C). The resulting turbid mixture was probe-sonicated for 120 sec (Sonicator Model W-220F, Heat Systems-Ultrasonics, Inc., Plainview, NY), and warmed above 45°C (12) to give an opalescent MLV suspension. DPPC was suspended as MLVs with similar heat/cool cycling without added sonication. Final lipid concentrations were verified by phosphate assay (13). Two hundred fifty μl of MLV suspension was sedimented onto aluminum foil substrates by centrifugation at 85,000 *g* for 3 h at 5°C in a specially designed sedimentation cell (14). The supernatant was discarded and the pellet was dehydrated overnight to 98% relative humidity (rh) at 8°C to facilitate fusion into membrane sheets (15, 16). For subsequent diffraction study, fused multilayer stacks of DEPN-8 or DPPC were mounted onto curved glass supports (17).

Differential scanning calorimetry (DSC)

DSC experiments used a DuPont 2910 Thermal Analysis System. Fused multilayer stacks of DEPN-8 or DPPC initially at 98% rh were subsequently equilibrated (3–3.5 h) to different fixed hydration levels in specially designed chambers at 4°C (D. Chester and B. Shnayder, unpublished results). Saturated salts used to control rh were: K_2SO_4 (95–98%), KNO_3 (88–96%), $ZnSO_4$ (93%), $Na_2C_4H_4O_6$ (91%), $[NH_4]_2SO_4$ (79–84%), NaCl (75%), or $NaNO_2$ (60–70%); the range of equilibrium rh between 0°C and 50°C for each salt is shown in parentheses (18). DSC scans were performed over the temperature range of 5 to 55°C at a rate of 2°C/min unless otherwise stated.

X-ray diffraction

Phase characteristics for DEPN-8 and DPPC were initially surveyed as a function of temperature and rh using small-angle X-ray diffraction to determine the average periodicity of the bilayer stacks (d, the unit cell repeat along the membrane stacking direction). An Elliott GX-18 rotating anode X-ray generator (Enraf-Nonius, Delft, The Netherlands) provided Cu K X-radiation that was focused on the detector face (300 μm FWHM at focus) in the horizontal direction with a home-built single Franks' mirror based on the original design (19). K_β radiation was filtered with Ni foil leaving K_α X-rays (λ = 1.54 Å), trimmed by beam-defining slits in the vertical direction to ~2 mm. Guard slits reduced parasitic scatter horizontally and vertically, and background scatter was reduced with He-filled beam paths. Lamellar scatter was recorded with a Braun one-dimensional quartz wire position-sensitive detector (PSD) (Innovative Technologies, Newburyport, MA) aligned along the horizontal axis parallel to the membrane stacking direction. The PSD was mounted on the 2θ axis of a 2-axis diffractometer, allowing precise determination of the number of detector channels as a function of 2θ. During data collection, samples were placed at the origin of the ϕ axis, with a specimen to detector distance of ~300 mm. Samples were aligned in the X-ray beam with the membrane planes oriented at grazing incidence with respect to the incident X-ray beam, followed by small adjustments to maximize the count rate of the diffracted signal. A tantalum beamstop was used to block the direct X-ray beam.

At the start of each diffraction study, multilayer samples were thermally annealed by three heat/cool cycles [just above 60°C, 15 min, room temperature], passing through

the gel to liquid-crystal transition temperature (T_m). Short X-ray exposures taken with the PSD during annealing demonstrated the expected phase changes (12), as well as a marked improvement in the coherent diffraction signal indicating that the samples were uniformly hydrated and reasonably well-ordered. For diffraction studies at fixed relative humidity, temperature was first lowered to the minimum value to be investigated, allowed to equilibrate, and an X-ray diffraction pattern was collected. Temperature was then raised, and the process was repeated. Prior to the change in relative humidity, the temperature was first raised above the L_α transition and a diffraction pattern was collected to assess sample stability. As noted earlier, rh for some of the saturated salts varies as a function of temperature. At the end of a typical experiment, DEPN-8 samples were equilibrated at 66% rh and 59.0°C, and were then re-equilibrated to 98% rh and 5-9°C prior to an additional X-ray exposure to assess stability and reversibility. Experiments with DEPN-8 were also conducted with the sample initially at the highest temperature, and sample temperature decreased during the course of the exposure sequence. Samples were allowed to equilibrate for ≥90 min between exposures. Three DEPN-8 and two DPPC samples were used in this study. Each sample was cycled through at least twice.

Diffraction data reduction

Raw data files from the PSD were transferred to a VAX 8250 (Digital Equipment Corporation, Maynard, MA) and reduced using a suite of small-angle scattering software developed at the University of Pennsylvania (V. Skita and R. Fischetti, unpublished results) and subsequently updated at the University of Connecticut (V. Skita, unpublished results). Data files were first corrected for detector uniformity and linearity. From a least square fit of the diffraction peak position (converted from channels to 2θ) versus peak index, d and $2\theta = 0$ (i.e., the reciprocal space origin) were determined. The final data were converted from 2θ to s ($s = 2\sin\theta/\lambda$).

Electron density profiles

Two-dimensional X-ray diffraction patterns were collected and analyzed to determine electron density profile structures. Complete lamellar and in-plane diffraction patterns were measured using X-ray film (Kodak DEF-5, Kodak, Rochester, NY). A specimen to detector distance of ~60 mm was used to detect both the high and low angle patterns simultaneously. The X-ray beam was focused in the horizontal direction as above, with the vertical height of the beam reduced to approximate point-focus. Film packets (two-four films) were mounted on the 2θ-axis of the 2-circle diffractometer. For calibration, a series of direct beam exposures of ~1 sec were taken at fixed intervals of 2θ, and the resulting film was digitized using the same parameters as the two-dimensional diffraction patterns. Exposure times for experiments measuring complete lamellar and in-plane scattering ranged from 18 to 24 h.

High resolution film patterns were digitized using an Optronics P-1700 scanner (Optronics, Chelmsford, MA) with a resolution of 100 μm. Lamellar scatter was radially integrated using a modified version of the "butterfly" integration algorithm developed at Princeton University (20). The integration parameters were chosen to totally encompass each reflection. Typical mosaic spread was 30-50°. The resultant one-dimensional function was background corrected using a cubic spline fit (21) and subsequently converted from channels to s to yield I(s). Data were indexed and the average periodicity was calculated as described above. Diffraction peaks were integrated to yield the integrated intensity, I(h), and Lorentz corrected (for a complete discussion see refs. 22, 23) by a factor of h to yield I'(h). Electron density profiles [$\varrho(z) = \int\int \varrho(x,y,z)dxdy$] were calculated over the range $z = \pm d/2$ according to the Fourier transform:

$$\varrho(z) = \sum_{h=1}^{h=h_{max}} \sqrt{I'(h)}\, \cos\left(2\pi z \frac{h}{d}\right) \Phi(h) \qquad \textit{Eq. 1)}$$

where h = diffraction order; h_{max} = the highest observed diffraction order; and $\phi(h)$ = cosine of the h*th* order phase [0 or π, for centrosymmetric $\varrho(z)$]. $\phi(h)$ was initially determined by physical reasonableness (24) as the number of non-zero reflections was small (4-5). As an additional test of our phase assignments, we required consistency among structure factors calculated for nearly isomorphous structures. The high angle regions of two-dimensional diffraction patterns were integrated radially to yield acyl chain spacing, and angularly to ascertain chain orientation with respect to the membrane stacking direction.

The structure factor F(s) was calculated from each electron density profile for DEPN-8 from the equation:

$$F(s) = \int_{-d/2}^{d/2} \varrho(z) \exp(2\pi i s z)\, dz \qquad \textit{Eq. 2)}$$

for $0 < s < h_{max}/d$). Note, $I'(h) = |F(s)|^2$ evaluated at $s = h/d$. Finally, $\phi(h)$ was evaluated for several data sets according to the method of Sayre (25).

RESULTS

The periodicity values of DPPC and DEPN-8 bilayers are summarized in **Table 1** and **Table 2,** respectively. The phase diagram for DPPC has been determined previously by several investigators using several different methods

TABLE 1. Summary of experimentally determined periodicities (Å) for DPPC

	Temperature °C											
%rh	5-9	10-14	15-19	20-24	25-29	30-34	35-39	40-44	45-49	50-54	55-59	60-64
95-98	59.7			59.5			58.0					51.8
91	58.6			58.6			58.0				51.7	
79-84	55.0			57.2			57.1			52.2		
75	56.8			57.2			57.1				51.4	
60-70	56.6							56.8				50.9

Periodicities have a maximum error of ± 0.5 Å.

(see ref. 5). Below its gel to liquid crystal transition temperature of 41-42°C, DPPC bilayers exhibited the expected periodicity (55-59 Å) and acyl chain behavior indicative of an $L_{\beta'}$ phase over a range of relative humidities (Table 1). In contrast, at temperatures below its T_m of ~45°C, DEPN-8 had repeat periods varying from ~42 Å to 58 Å, with the smaller repeat consistent with an interdigitated phase (Table 2). This interdigitated phase for DEPN-8 bilayers below T_m existed at high relative humidities, and disappeared as humidity was lowered to ~85% or below (Table 2). Above T_m both DEPN-8 and DPPC bilayers exhibited the reduced periodicity of 51-52 Å characteristic of the L_α phase (Tables 1, 2).

Characteristic one-dimensional diffraction patterns for DEPN-8 in the interdigitated lamellar phase (L_{int}), gel-crystalline phase (L_β), or liquid-crystalline phase (L_α) are shown in **Fig. 1.** Figure 1A (95-98% rh, t = 15.0°C) is a typical diffraction pattern for L_{int}, with a periodicity of 46.5 Å. Note the absence of a fourth order, and the presence of a relatively strong third order. The diffraction peaks are sharp, and show almost no broadening as h increases, indicative of very little lattice disorder (for a complete discussion of disorder, see ref. 22). In Fig. 1B (95-98% rh, t = 26.6°C), DEPN-8 is still in L_{int} with a periodicity of 44.6 Å. The pattern is very similar to Fig. 1A, except that a small fourth order is observed.

Figure 1C (95-98% rh, t = 36.8°C) shows a more complicated diffraction pattern for DEPN-8, with numerous peaks indicative of multiple phases. The overall pattern shows both L_β and interdigitated gel phases. Peaks 1a, 2a, 3a, 4a arise from a 56.9 Å lattice (L_β); peaks 1b, 2b, 3b from a 40.8 Å lattice (L_{int}); peaks 1c, 2c, 3c, 4c from a 60 Å lattice (L_β); and peaks 1d, 3d from a 45 Å lattice (L_{int}). Peak 1c is a small shoulder on the low angle side of peak 1a, and peaks 2b, 3c and 3c, 4c could not be resolved from each other. A predicted peak (2d) at 0.0444 A^{-1} was also not observed and two peaks at 0.0385 and 0.0602 A^{-1} (arrows) could not be indexed.

Figure 1D (95-98% rh, t = 43.6°C) shows DEPN-8 just below its T_m. The sample is phase separated, with the majority of bilayers typical of the L_β phase and a periodicity of 57.2 Å. Peaks 1-4 arise from this lattice, with a strong fourth order and relatively weak second and third order. All diffraction orders are sharp indicating negligible lattice disorder. Peak 1' and 4' index at 49.9 Å and are indicative of a small fraction of coexisting L_α phase.

Figure 1E (95-98% rh, t = 45.6°C), just above the T_m of DEPN-8, is a typical diffraction pattern for an L_α phase with a periodicity of 51.8 Å. The second and third orders are increased in magnitude compared to DEPN-8 in the L_β phase (Fig. 1D). The diffraction peaks are

TABLE 2. Summary of experimentally determined periodicities (Å) for DEPN-8

	Temperature °C											
%rh	5-9	10-14	15-19	20-24	25-29	30-34	35-39	40-44	45-49	50-54	55-59	60-64
95-98	46.9	46.5			44.6		58/41	57/50	51.8		51	
91	44.5			43.1							50.9	
79-84	59.6	59.2				<58>			52.4		50.7	
75	59.4				58.7				<57>		51	50.6
60-70	58.2				57.8			57.4			51.4	

When two numbers are given, the second represents the periodicity of a significant second phase. Numbers in brackets represent the average periodicity for multiple domains in one phase. Periodicities have a maximum error of ± 0.5 Å.

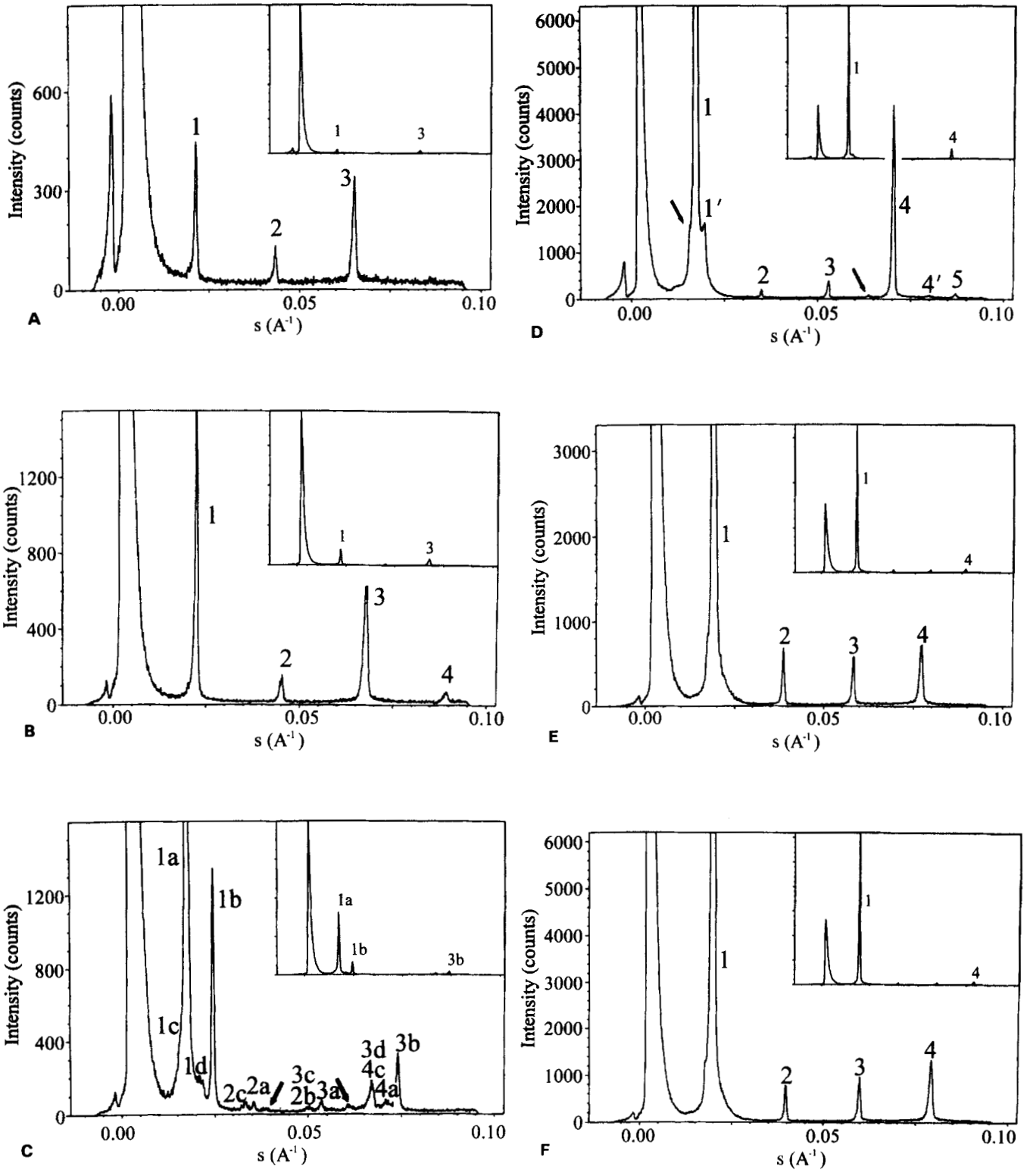

Fig. 1. Diffraction patterns for phosphonolipid DEPN-8 at 98% rh. From the least square fit of the diffraction peak position versus peak index, both d and I(0) were determined. The abscissa has been converted to reciprocal Angstroms (A^{-1}) for clarity. Note, I(s) = I(h/d), where d is the periodicity of a given lattice, and h is the peak index (i.e., diffraction order number). The diffraction patterns shown in the figure have not been Lorentz corrected. The intensity around I(0) is due to parasitic scatter from the beamstop. The insert has been scaled 20× in panel A, and 10× in panels B–F. A) Temperature equal to 15.0°C, B) 26.6°C, C) 36.9°C, D) 43.6°C, E) 45.6°C, and F) 55.3°C. Artifacts due to diffraction of K_β X-rays from the 57.2 Å lattice due to incomplete K_β filtration are shown by the arrows in D), while the shoulder at 0.0175 A^{-1} is due diffraction of K_β X-rays from the 51.8 Å lattice in E), and the shoulder at 0.0178 A^{-1} is due to diffraction of K_β X-rays from the 51.0 Å lattice in F).

sharp, and show almost no broadening as h increases, indicative of minimal lattice disorder. Figure 1F (95–98% rh, t = 55.3°C) is a similar L_α diffraction pattern for DEPN-8 with a periodicity of 51.0 Å.

Figure 2 is a composite of the two-dimensional film pattern for DEPN-8 at 98% rh and 7.8°C (panel A) and 24°C (panel B). Both the low angle lamellar (vertical arcs along the horizontal axis) and high angle equatorial data (arc with its "maxima" at the top and bottom of the figure) are apparent. In the diffraction pattern in panel A, note the absence of h = 4, 6–8 along the lamellar axis. A small amount of the sample has phase separated into the 42 Å L_{int} phase as evidenced by a small arc between h = 3 and 5, and the small arc on the high angle side of h = 9. These arcs index as h = 4 and 8 of a 42 Å lattice. The occurrence of this minor lattice did not affect the data reduction and analysis. The pattern in panel B does not appear phase separated, with h = 1-5, 9 clearly visible. The equatorial diffractions from both panels are discussed below.

Electron density profiles were determined for DEPN-8 as a function of temperature at 95–98% rh from the two-

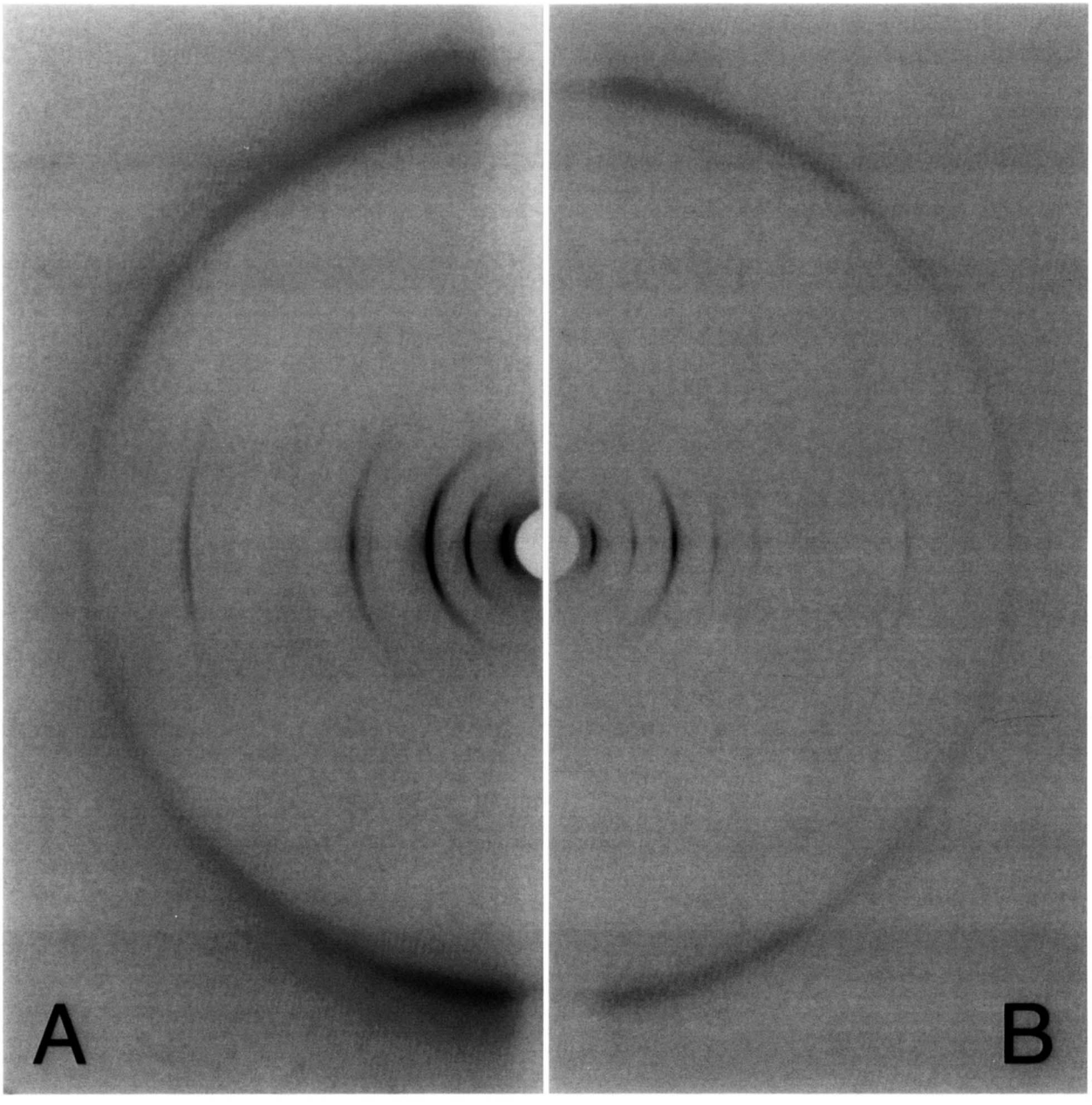

Fig. 2. Typical two-dimensional diffraction patterns collected on X-ray film. The two-dimensional X-ray diffraction pattern for DEPN-8 at 7.8°C (A, left) and 24.0°C (B, right) are shown in the composite photograph. Both the low and high angle diffraction are visible. The hole in the center is the shadow of the beamstop.

dimensional X-ray diffraction studies (**Fig. 3**). The integrated intensities [I(h)] and their corresponding phases [ϕ(h)] (see Methods) are shown in **Table 3.** I(h) and ϕ(h) are used to calculate ϱ(z) for DEPN-8 at 95–98% rh and 7.8, 24.0, and 31.1°C according to equation 1. The terminology used to describe the anatomy of membrane bilayers has been clarified by Wiener and White (26) and has been recently reviewed by White and Wimley (27). With this in mind, the inter-bilayer waterspace is observed for $d/2 > |z| > \sim 18.0$ Å, the phosphonolipid headgroup is observed from $\sim 18.0 > |z| > \sim 13.5$ Å, the glycerol backbone is observed from $\sim 13.5 > |z| > \sim 9.5$ Å, the acyl chain region from $|z| < \sim 9.5$ Å, with the bilayer center at 0 Å, in Fig. 3. The electron dense features at ±15.25, ±15.45 and ±15.55 Å (corresponding to the 7.8, 24.0, and 31.1°C electron density profiles, respectively) are interpreted as the centers of mass of the phosphonolipid headgroups. Thus, the distance between the phosphonolipid headgroup region of the DEPN-8 bilayers are 30.5, 30.9, and 31.1 Å for the 7.8, 24.0, and 31.1°C bilayers, respectively. The profiles show a marked increase in electron density in the interior 10 Å of the bilayer. This clearly demonstrates that the acyl chains of opposing membrane leaflets are interdigitated in the interior of the membrane.

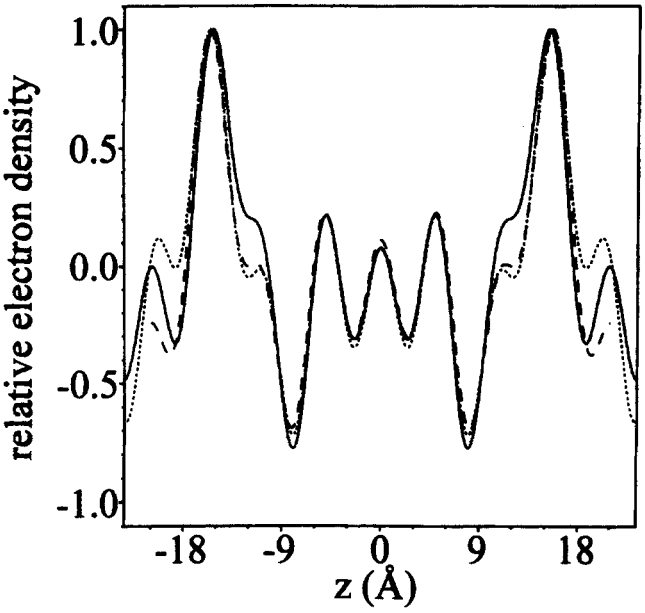

Fig. 3. Electron density plot for DEPN-8. Figure shows the electron density profiles for DEPN-8 at 98% rh at 7.8°C (solid line), 24.0°C (short dash), and 31.1°C (long dash). Profiles were normalized to set the largest electron density feature to 1.0; scale factors for ϱ(z) at 7.8, 24.0, and 31.1°C were 1.064, 1.081, and 0.919, respectively. Additionally, ϱ(z) was "contrast" adjusted so that $\Sigma\varrho(z) = 0$ (always <0.75%).

Structure factors (**Fig. 4**) were calculated for DEPN-8 at 95–98% rh and 7.8, 24.0, and 31.1°C according to equation 2 to evaluate our phase assignments (Table 3). As illustrated, $F(s)_{7.8°C}$ and $F(s)_{24.0°C}$ are very similar. This indicates that the two electron density profiles are very similar, almost isomorphous, save for the waterspace (28). $F(s)_{31.1°C}$ substantially differs from $F(s)_{7.8°C}$ and $F(s)_{24.0°C}$ for $0.11 < s < 0.17$ A^{-1}. Note, however, that $\varrho(z)_{31.1°C}$ differs substantially from $\varrho(z)_{7.8°C}$ and $\varrho(z)_{24.0°C}$ only in the waterspace region of the electron density profile. Electron density profiles calculated by sampling $F(s)_{7.8°C}$ at $h/d_{24.0°C}$ and sampling $F(s)_{24.0°C}$ at $h/d_{7.8°C}$ are very similar (data not shown) and demonstrate that these two structures share the same F(s). Note, $F(s)_{24.0°C}$ nearly predicts the extinction of $I'(4)_{7.8°C}$. The structure factors for DEPN-8 at 95–98% rh and 7.8, 24.0, and 31.1 are totally consistent with the assignment of ϕ(h) as −1, −1, +1, −1, −1, ±1, ±1, +1, +1 for h = 1,9. If ϕ(5) is changed to +1 the following observations are made (calculations not shown). First, $F(s)_{24.0°C}$ does not predict the extinction of $I'(4)_{7.8°C}$. Second, there is poor agreement between the two structure factors for $0.08 < s < 0.13$ A^{-1}. Third, the electron density profiles calculated are neither isomorphous nor physically interpretable based on the known electron densities of bilayer headgroups and

TABLE 3. Summary of integrated intensities for DEPN-8

	Temperature	7.8°C	24.0°C		31.1°C	
	Periodicity	46.9 Å	46.5 Å		41.9 Å	
	Resolution[a]	5.2 Å	5.2 Å		5.2 Å	
Order (h)	I(h) (counts)	ϕ(h)	I(h) (counts)	ϕ(h)	I(h) (counts)	ϕ(h)
1	1.84×10^4	−1	8.71×10^3	−1	1.00×10^4	−1
2	2.35×10^4	−1	2.30×10^3	−1		
3	6.02×10^4	1	1.57×10^4	1	1.29×10^4	1
4			1.89×10^3	−1	8.27×10^3	−1
5	1.65×10^4	−1	1.17×10^3	−1		
6						
7						
8					2.67×10^3	1
9	9.95×10^3	1	2.38×10^3	1		

[a]Resolution, calculated by dividing the periodicity by h_{max}.

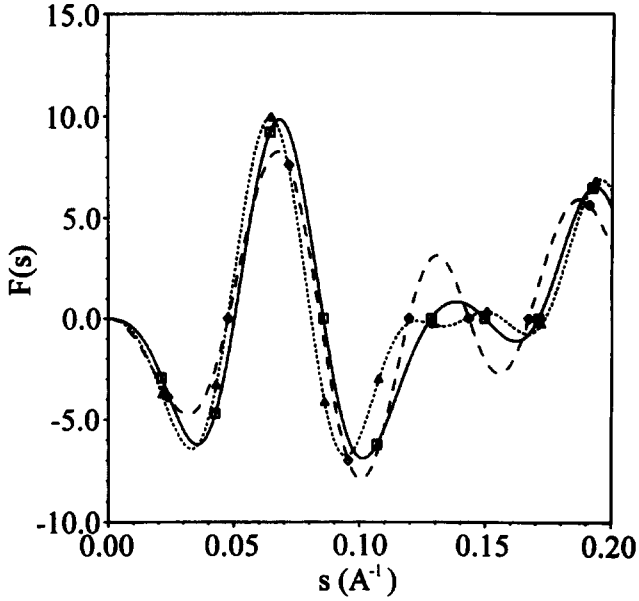

Fig. 4. Structure factor plot for DEPN-8. Structure factor plots for DEPN-8 at 98% rh at 7.8°C (solid line), 24.0°C (short dash), and 31.1°C (long dash) are shown. The structure factor plots are tagged at s = h/d by squares (7.8°C), triangles (24.0°C), and diamonds (31.1°C). The contrast adjustment forces F(0) = 0, and compensates for artifacts introduced by the normalizing $\varrho(z)$.

acyl chains. For instance, $\varrho(z)_{7.8°C}$ predicts an electron dense feature in the center of the bilayer with nearly equal magnitude to the phosphonolipid headgroup, and $\varrho(z)_{24.0°C}$ predicts an electron dense feature in the center of the bilayer with about half the magnitude to the phosphonolipid headgroup.

High angle scatter indicative of in-plane acyl chain packing was observed at or near the equator at 0.0 ± 10°, for the interdigitated phase. This demonstrates that there is no appreciable acyl chain tilt in the L_{int} phase, thus warranting the nomenclature $L_{\beta i}$. A strong maxima is observed at 1/4.1 A^{-1}, and a broad shoulder at 1/4.3 A^{-1} at 31.1°C (**Fig. 5**). At 24.0°C the 1/4.3 A^{-1} shoulder has been replaced by an even broader shoulder at 1/4.4 A^{-1}, and a hint of a shoulder at 1/3.8 A^{-1} (Figs. 2, 5). The maxima at 1/4.1 A^{-1} is still present. At 7.8°C the shoulder at 1/3.8 A^{-1} is pronounced and broad (Figs. 2, 5). The 1/4.4 A^{-1} is reduced somewhat, and the maxima at 1/4.1 A^{-1} is still observed.

Calorimetric measurements were made on oriented multilayer stacks of DEPN-8 and DPPC as a function of rh, to correlate lyotropically induced thermal phase behavior with the X-ray scattering results and to confirm full lipid hydration conditions (D. Chester and B. Shnayder, submitted for publication). **Figure 6A, B** shows representative calorimetric scans for DEPN-8 under different hydration conditions. DSC on DEPN-8 MLV in solution reveal a first order kinetic transition with a T_m and ΔH_c of 44.99 ± 0.08°C and 61.97 ± 3.22 J/g [10.16 Kcal/mol], respectively (Fig. 6A). There was no evidence of either a pretransition or subtransition event. Heating and cooling scans on these vesicles demonstrated the anticipated hysteresis observed for the lipid gel state melting and a single first order renucleation process. A first order kinetic transition with a T_m = 40.94 ± 0.22°C and ΔH_c = 43.94 ± 3.13 J/g [7.71 Kcal/mol] was observed for DPPC, respectively. A pretransition at T_{mp} = 36.39 ± 0.27°C and ΔH_p = 6.73 ± 1.02 J/g [1.18 Kcal/mol] was also noted for DPPC. These numbers compare favorably with values reported in the literature (29).

The lyotropic effects on DEPN-8 oriented multilayer thermal phase behavior are shown in Fig. 6A, B, with each sample maintained at a fixed water:lipid ratio during the course of a calorimetric scan. In these experiments, it is important to remember that the samples are "trapped" at a fixed water:lipid ratio at 4°C. This differs somewhat from X-ray methods where the samples are subject to temperature-dependent changes in both rh and absolute water vapor pressure. Partial multilayer dehydration from 98 to 88% rh caused an initial 2°C decrease in the DEPN-8 main chain transition from 44.34°C (98% rh) to 42.33°C (88% rh). This is in contrast to DPPC dispersions, which demonstrate an upward progression in main chain transition temperature with decreased hydration (5, 30, 31). Recently D. Chester and B. Shnayder (unpublished results) have reported the same behavior for partially hydrated, oriented DPPC multilayers. The multilayer transitions occurring for DEPN-8 at high hydration (98 and 96% rh, Fig. 6A) are clearly first order processes while the transition at 93% rh is no longer first order and

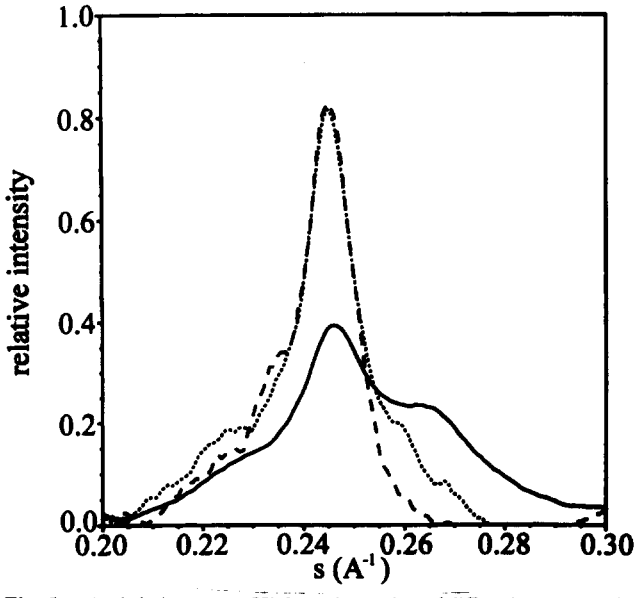

Fig. 5. Acyl chain scatter. High angle portion of diffraction pattern for DEPN-8 at 98% rh at 7.8°C (solid line), 24.0°C°C (short dash), and 31.1°C (long dash) are shown.

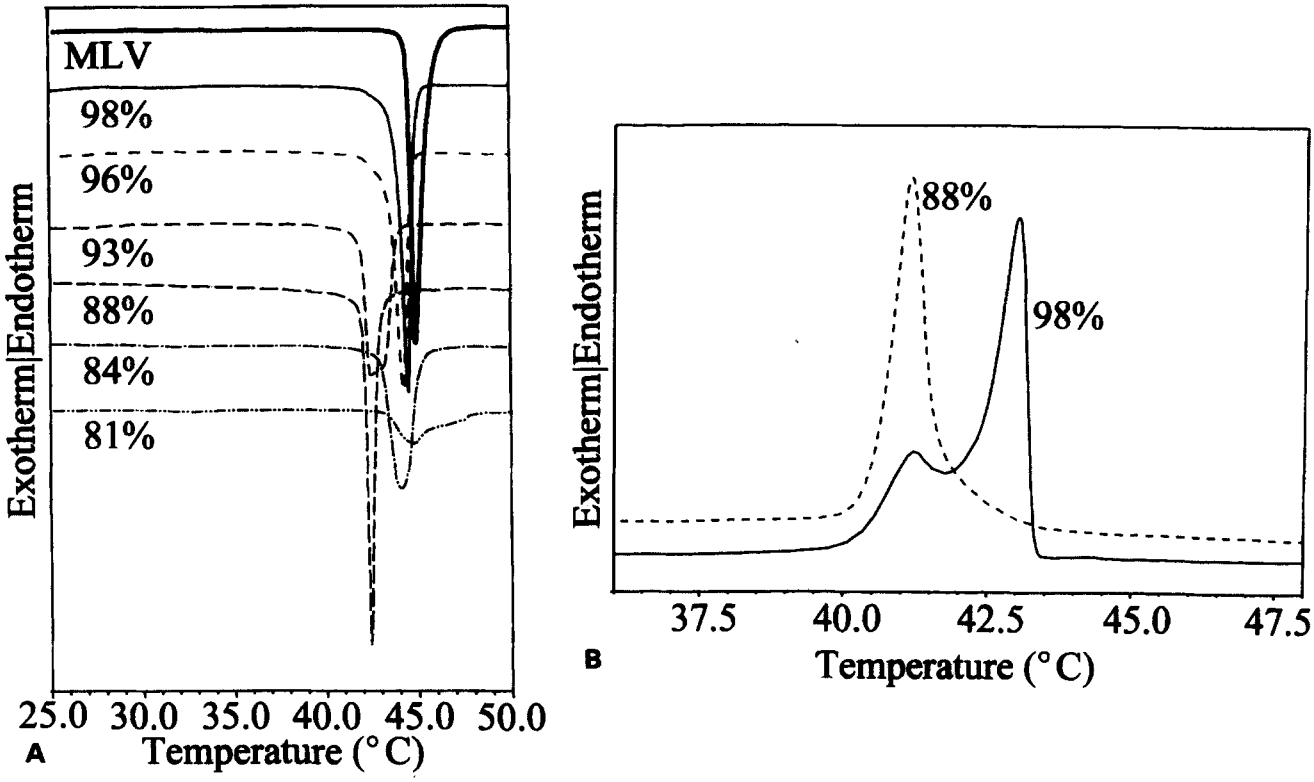

Fig. 6. Calorimetry. A) Representative heating scans for DEPN-8 MLVs in excess solvent (thick line) and multilayers stacks as a function of equilibrium hydration over saturated salt solutions (81-98% rh) at 4°C. B) DEPN-8 cooling scans for multilayers at 98 and 88% rh.

resulted in a shift in T_m to 42.40°C. Further dehydration to 88% rh gave a recurring first order transition main chain transition at 42.33°C. There was also a slight decrease in transition enthalpy from 59.58 ± 5.19 to 50.23 ± 2.99 J/g through this hydration range. Dehydration to 84% rh resulted in a broadened first order transition at 44.24°C and decrease in enthalpy to 47.27 ± 3.86 J/g. At approximately 81% rh, the thermal phase transition was no longer a first order kinetic process, as indicated by both transition broadening and observation of a higher temperature hump, and enthalpy decreased to approximately 20 J/g. As the multilayer samples were dehydrated to hydration levels significantly below the bound/free water transition region, the transition moved to very high temperatures [66°C] with indications of significant changes to the lipid.

Figure 6B illustrates the cooling scans for DEPN-8 multilayers at 98% and 88% rh, respectively. The DEPN-8 transition upon cooling at 98% rh had two renucleation maxima at 43.01 and 41.26°C. Interestingly, the cooling transitions observed for both for DEPN-8 MLVs (not shown) and multilayers dehydrated to 88% rh were sharp first order transitions occurring at 41.26°C. The second higher temperature transition found for the 98% rh sample (and for 96 and 93% rh, not shown) was presumably related to inhomogeneity in the $L_\alpha \rightarrow L_\beta$ transition as a function of substrate or DSC pan surface interaction.

DISCUSSION

In the present study, X-ray diffraction and differential scanning calorimetry were used to probe the bilayer and thermal behavior of a synthetic diether phosphonolipid analog (DEPN-8) of the primary lung surfactant glycerophospholipid DPPC. Results showed that in contrast to DPPC, DEPN-8 formed interdigitated bilayers at temperatures below its gel to liquid crystal transition at high relative humidity (Tables 1, 2). Electron density profiles and structure factor plots were also constructed for DEPN-8 from complete assessments of lamellar and in plane scatter, further defining the interdigitated state (Table 3, Figs. 3-5). Also, DSC results clearly demonstrated and corroborated the acyl chain behavior and bilayer transitions observed in our X-ray scattering experiments under the higher hydration conditions.

Bilayer periodicity for any phospholipid is a function of hydration, headgroup orientation, and acyl-chain packing. DEPN-8 can be in one of three major phases depending on temperature and hydration (Table 2, Fig. 1). At low temperatures and high hydration, DEPN-8 bilayers ap-

pear to be interdigitated, with a characteristic periodicity of 42–46 Å (Tables 2, 3, Figs. 1A, B). The diffraction pattern for DEPN-8 under these conditions is characteristic of interdigitated lipids (32, 33), with a strong third order and a nearly absent fourth order. At lower hydration and temperature below T_m, DEPN-8 diffraction patterns were characteristic of an L_β phase, with a periodicity of 57–59 Å (Table 2). Finally, above T_m DEPN-8 was in the L_α phase with a periodicity of 51 Å regardless of hydration (Table 2, Figs. 1E, F). The diffraction patterns of DEPN-8 in non-interdigitated phases were very similar to DPPC in the corresponding phases. Under appropriate conditions near the phase transition, multiple domains were observed with DEPN-8 exhibiting both the L_{int} and L_β phases (Fig. 1C) or the L_β and L_α phases (Fig. 1D).

The phase choices (h = 1–9 of π, π, 0, π, π, $0/\pi$, $0/\pi$, 0, 0) found here for DEPN-8 are the same for all forms of L_{int} and are in complete agreement with those of Kim, Mattai, and Shipley (32, 33) under conditions of high hydration for the ether-linked phospholipid, dihexadecyl phosphatidylcholine (DHPC) at 22°C. For DHPC, Kim et al. (32, 33) did not report a phase for h = 4, 8, and 9. The acyl chains are not appreciably tilted, with the majority of acyl chains aligned (on average) along the normal to the bilayer plane. The acyl chain spacing at 1/4.1 A^{-1} and the pronounced shoulder at 1/3.8 A^{-1} at 7.8°C (but not at 24.0 or 31.1°C) found here for DEPN-8 is also consistent with previous work on DHPC (34). As with DHPC (34), the acyl chain scatter of DEPN-8 at 24.0°C, and even more so at 31.1°C, with its sharp single component, is indicative of non-tilted two-dimensional hexagonal lattice (35). In contrast, the acyl chain scatter observed for $L_{int,\ 7.8°C}$, with the addition of a broad 1/3.8 A^{-1} feature, is indicative of a non-tilted orthorhombic subphase (35). The X-ray diffraction presented here clearly indicates a $L_{int,\ 7.8°C} \rightarrow L_{int,\ 31.1°C}$ subtransition. Interestingly, under no conditions could we observe this subtransition calorimetrically. As the observed calorimetric subtransitions are notably scan rate-dependent (34, 36), this is one potential rationale for its absence in heating and cooling scans.

The structure of DEPN-8 bilayers as deduced from the electron density profiles (Fig. 3) demonstrates that the ~30 Å headgroup–headgroup spacing is invariant from 7.8°C to 31.1°C, as is the structure of the acyl chain region. The major changes in the profile structure with increased temperature from 7.8°C to 31.1°C occurs in the waterspace. At 31.1°C, the bilayer appears less hydrated than at the lower temperatures as evidenced by the decrease in electron density at the edge of the unit cell (Fig. 3), and there is also a general decrease in bilayer periodicity in the L_{int} phase as the temperature is increased (Table 2). At 7.8°C an electron dense feature at $|z|$ ~11 Å is probably due to orientational differences in the phosphonolipid headgroup (Fig. 3). At 7.8°C the headgroup–headgroup spacing was about 1 Å less than for 24.0°C and 31.1°C (Fig. 3), possibly due to orientational differences of the headgroup below the subtransition. Our X-ray data have a higher resolution (5.2 Å) than previous studies of ether-linked phospholipids (32–34), at least partly due to the increased signal to noise ratio found in diffraction arcs of oriented multilayer stacks compared to the rings seen in unoriented multilayer vesicles. By orienting our samples, a direct measurement of the acyl chain tilt was also possible.

Although the bilayer behavior of DEPN-8 was very similar to that found earlier for DHPC (32–34, 36), some differences did exist in thermal properties. While the main chain thermal phase transitions of DHPC and DEPN-8 are similar, 44.2 versus 44.99°C for MLV preparations, the calorimetric phase behavior is strikingly dissimilar. In our DSC experiments with DEPN-8 there was no observation of either subtransitional or pretransitional events, in agreement with the work of Lu et al. (12). DHPC, on the other hand, elicits clear sub and pretransitions that can be observed both on heating and cooling (34, 36). Also, our DSC results with DEPN-8 clearly demonstrate a decreased transition temperature upon initial dehydration to the range of 88% rh (Fig. 6). The studies of Kim et al. (32) demonstrate that upon dehydration, the DHPC transition processes smoothly to a limiting temperature of 74.2°C at 4.8% water or approximately 2 waters/lipid.

The ether linkage in DEPN-8 is most likely the dominant factor in its ability to form interdigitated bilayers in contrast to ester-linked DPPC. Only under extreme conditions of high pressure (37) has pure DPPC been observed to form interdigitated bilayers. Several laboratories have investigated the formation of solute-induced interdigitated phases for DPPC, including systems with cychlohexanol (38), n-butanol (39), and ethanol (40–43). However, under physiological conditions, DPPC does not appear to interdigitate. The DHPC and DPPC molecules differ solely in the ether versus ester linkage group at the chain–backbone junction, showing that this structural property alone can give rise to L_{int}. The electron density profile structures reported for DHPC (32–34) under similar conditions of hydration and temperature, are very similar to those observed here. This indicates that changing the headgroup phosphate in DHPC to a phosphonate in DEPN-8 does not effect the formation of intergiditated bilayers by the respective molecules.

Glycerolipids esters possess a hydrogen-accepting group for hydrogen bonding, but lack a hydrogen-donating group in the glycerol–backbone region (44). In contrast, glycerolipid ethers completely lack the ability to from hydrogen bonds in glycerol–backbone region. This in turn may lead to the greater hydrophobicity observed in ether-linked phospholipids when compared to ester-linked phospholipids. This affects a number of molecular

properties including lower hydration (44) and closer acyl chain packing (36) in glycerolipid ethers. The ether linkage also has a more flexible and mobile character than the ester linkage (45). The disappearance of interdigitated bilayers for DEPN-8 at lower relative humidities (below about 90% rh at low temperature in Table 2) suggests that a minimum limit of overall headgroup hydration is necessary to allow the interdigitated bilayer form to be stable, although decreased hydration in the chain-backbone region (in ether-linked versus ester-linked compounds) favors interdigitation.

The ability of DEPN-8 to form interdigitated bilayers may be important for its previously defined differences in surface activity compared to DPPC. Both DEPN-8 and DPPC can generate extremely low surface tensions in dynamically compressed films at the air-water interface at temperatures below their L_α phase transition (6, 7, 9, 10). This behavior can be correlated, in part, with their fully saturated and equivalent C_{16} length acyl chains. However, DEPN-8 has considerably more rapid adsorption and better film respreading than DPPC (7, 9, 10). The fact that DHPC also exhibits improved respreading over DPPC in dynamically cycled films at the air-water interface at room temperature (9, 10) further suggests that the ether linkage is more important than the phosphate/phosphonate group in this surface behavior.

In summary, X-ray diffraction has been used to evaluate the phase behavior of DEPN-8, a diether phosphonolipid analog of DPPC. DPPC and DEPN-8 formed similar lamellar assemblies at all humidities (66–98%) above the L_α phase transition temperature, and at low relative humidity below the liquid crystal transition. However, at high humidity for temperatures below the liquid crystal transition, DEPN-8 formed interdigitated bilayers, which may be related to the surface property differences (enhanced adsorption and film dynamic respreading) that this molecule exhibits compared to DPPC.

The authors would like to thank Dr. Robert Sweet of the Structural Biology Department, Brookhaven National Laboratory, Upton, New York for use of his Optronics film scanner. This work was supported in part by the National Institutes of Health through grants HL-45284 (University of Connecticut) and Pulmonary SCOR, HL-36543 (University of Rochester), and Council for Tobacco Research Award, SA-009 (Dr. Skita).

Manuscript received 11 October 1994 and in revised form 18 January 1995.

REFERENCES

1. Shapiro, D. L., and R. H. Notter. 1989. Surfactant Replacement Therapy. A R. Liss, Inc., New York.
2. Robertson, B., L. M. G. van Golde, and J. J. Batenburg. 1992. Pulmonary Surfactant. From Molecular Biology to Clinical Practice. Elsevier Publishers, Amsterdam, The Netherlands.
3. Notter, R. H., and J. N. Finkelstein. 1984. Pulmonary surfactant: an interdisciplinary approach. *J. Appl. Physiol.* **57:** 1613–1624.
4. Notter, R. H. 1989. Physical chemistry and physiological activity of pulmonary surfactants. *In* Surfactant Replacement Therapy. D. L. Shapiro and R. H. Notter, editors. A. R. Liss, Inc., New York, NY. 19–70.
5. Small, D. M. 1986. Phospholipids. *In* The Physical Chemistry of Lipids. From Alkanes to Phospholipids. Handbook of Lipid Research, Vol. 4. D. M. Small, editor. Plenum Press, New York. 475–522.
6. Turcotte, J. G., A. M. Sacco, J. M. Steim, S. A. Tabak, and R. H. Notter. 1977. Chemical synthesis and surface properties of an analog of the pulmonary surfactant dipalmitoylphosphatidylcholine. *Biochim. Biophys. Acta.* **488:** 235–248.
7. Turcotte, J. G., W. H. Lin, P. E. Pivarnik, A. M. Sacco, M. S. Bermel, R. Z. Lu, and R. H. Notter. 1991. Chemical synthesis and surface activity of lung surfactant phospholipid analogs: II. Racemic N-substituted diether phosphonolipids. *Biochim. Biophys. Acta.* **1084:** 1–12.
8. Turcotte, J. G., W. H. Lin, N. C. Motola, P. E. Pivarnik, N. N. Bhongle, H. R. Heyman, R. Z. Lu, and R. H. Notter. 1991. Chemical synthesis and surface activity of lung surfactant phospholipid analogs. III. Chiral N-substituted ether-amide phosphonolipids. *Chem. Phys. Lipids.* **48:** 81–95.
9. Liu, H., J. G. Turcotte, and R. H. Notter. 1994. Dynamic interfacial properties of surface-excess films of phospholipids and phosphonolipid analogs: I. Effects of pH. *J. Colloid Interface Sci.* **167:** 378–390.
10. Liu, H., J. G. Turcotte, and R. H. Notter. 1994. Dynamic interfacial properties of surface-excess films of phospholipids and phosphonolipid analogs: II. Effects of chain linkage and headgroup structure. *J. Colloid Interface Sci.* **167:** 391–400.
11. Touchstone, J. C., J. C. Chen, and K. M. Beaver. 1980. Improved separation of phospholipids by thin-layer chromatography. *Lipids.* **15:** 61–62.
12. Lu, Z. R., J. G. Turcotte, W. H. Lin, J. M. Steim, and R. H. Notter. 1992. Differential scanning calorimetry studies of phosphonolipid analogs of lung surfactant glycerophospholipids. *J. Colloid Interface Sci.* **154:** 24–34.
13. Chester, D. W., L. G. Herbette, P. R. Mason, A. F. Joslyn, D. J. Triggle, and D. E. Koppel. 1986. Diffusion of dihydropyridine calcium channel antagonists in cardiac sarcolemmal lipid multibilayers. *Biophys. J.* **52:** 1021–1030.
14. Blasie, J. K., C. R. Worthington, and M. M. Dewey. 1969. Molecular localization of frog retinal receptor photopigment by electron microscopy and low-angle diffraction. *J. Mol. Biol.* **39:** 407–416.
15. Clark, N. A., K. J. Rothschild, D. A. Luippold, and B. A. Simon. 1980. Surface-induced lamellar orientation of multilamellar membrane arrays. Theoretical analysis and a new method with application to purple membrane fragments. *Biophys. J.* **31:** 65–96.
16. Herbette, L., A. Scarpa, J. K. Blasie, C. T. Wang, A. Saito, and S. Fleischer. 1981. Comparison of the profile structures of isolated and reconstituted sarcoplasmic reticulum membranes. *Biophys. J.* **36:** 47–72.
17. Herbette, L. G., J. Marquardt, A. Scarpa, and J. K. Blasie. 1977. A direct analysis of lamellar X-ray diffraction from hydrated oriented multilayers of fully functional sacroplasmic reticulum. *Biophys. J.* **20:** 245–271.
18. Spencer, H. M. 1926. *In* International Critical Tables of Numerical Data, Physics, Chemistry, and Technology. Vol.

1. E. W. Washburn, C. J. West, N. E. Dorsey, F. R. Bichowsky, and A. Klemenc, editors. McGraw-Hill Book Co., Inc., New York. 67–68.
19. Franks, A. 1955. An optically focusing X-ray diffraction camera. *Proc. Phys. Soc. B.* **68:** 1054–1064.
20. Gruner, S. M., T. B. Barry, and G. T. Reynolds. 1982. X-ray diffraction analysis of wet isolated bovine rod outer segment disks. *Biochim. Biophys. Acta.* **690:** 187–198.
21. Press, W. H., B. P. Flannery, S. A. Teukolsky, and W. T. Vetterling. 1988. Numerical Recipes in C. Cambridge University Press, Cambridge, U.K. 94–98.
22. Hosemann, R., and S. N. Bagchi. 1962. Direct Analysis of Diffraction by Matter. North-Holland Publishing Company, Amsterdam, The Netherlands.
23. Hukins, D. W. L. 1981. X-Ray Diffraction by Disordered and Ordered Systems. Pergamon Press, Oxford, U.K.
24. Luzzati, V., A. Tardieu, and D. Taupin. 1972. A pattern recognition approach to the phase problem: application to the X-ray diffraction study of biological membranes and model systems. *J. Mol. Biol.* **64:** 269–286.
25. Sayre, D. 1953. Some implications of a theorem due to Shannon. *Acta Cryst.* **5:** 843.
26. Wiener, M. C., and S. H. White. 1991. Fluid bilayer structure determination by the combined use of X-ray and neutron diffraction. I. Fluid bilayer models and the limits of resolution. *Biophys. J.* **59:** 162–173.
27. White, S. H., and W. C. Wimley. 1994. Peptides in lipid bilayers: structural and thermodynamic basis for partitioning and folding. *Curr. Opin. Struct. Biol.* **4:** 79–86.
28. Moody, M. F. 1963. X-ray diffraction pattern of nerve myelin: a method for determining the phases. *Science.* **142:** 1173–1174.
29. Marsh, D. 1990. CRC Handbook of Lipid Bilayers. CRC Press, Inc. Boca Raton, Florida. 139–140.
30. Kodama, M., M. Kuwabara, and S. Seki. 1982. Successive phase-transition phenomena and phase diagram of the phosphatidylcholine-water system as revealed by differential scanning calorimetry. *Biochim. Biophys. Acta.* **689:** 567–570.
31. Kodama, M. 1986. Phase-transition phenomena induced by the successive appearances of new types of aggregation states of water-molecules in the L-dipalmitoylphosphatidyl choline water-system. *Thermochim. Acta.* **109:** 81–89.
32. Kim, J. T., J. Mattai, and G. G. Shipley. 1987. Gel phase polymorphism in ether-linked dihexadecylphosphatidylcholine bilayers. *Biochemistry.* **26:** 6592–6598.
33. Kim, J. T., J. Mattai, and G. G. Shipley. 1987. Bilayer interactions of ether- and ester-linked phospholipids: dihexadecyl- and dipalmitoylphatidylcholines. *Biochemistry.* **26:** 6599–6603.
34. Ruocco, M. J., D. J. Siminovitch, and R. G. Griffin. 1985. Comparative study of the gel phases of ether- and ester-linked phosphatidylcholines. *Biochemistry.* **24:** 2406–2411.
35. Tardieu, A., V. Luzzati, and F. C. Reman. 1973. Structure and polymorphism of the hydrocarbon chains of lipids: a study of lecithin-water phases. *J. Mol. Biol.* **75:** 711–733.
36. Ruocco, M. J., A. Makriyannis, D. J. Sminovitch, and R. G. Griffin. 1985. Deuterium NMR investigation of ether- and ester-linked phosphatidylcholine bilayers. *Biochemistry.* **24:** 4844–4851.
37. Peng, X., and J. Jonas. 1992. High-pressure ^{31}P NMR study of dipalmitoylphosphatidylcholine bilayers. *Biochemistry.* **31:** 6383–6390.
38. Roth, L. G., and C. H. Chen. 1992. Thermodynamic elucidation of solute-induced lipid interdigitation phase: lipid interactions with hydrophobic versus amphipathic species. *Arch. Biochem. Biophys.* **296:** 207–213.
39. Zhang, F., and E. S. Rowe. 1992. Titration calorimetric and differential scanning calorimetric studies of the interactions of *n*-butanol with several phases of dipalmitoylphosphatidylcholine. *Biochemistry.* **31:** 2005–2011.
40. Boni, L. T., S. R. Minchey, W. R. Perkins, P. L. Ahl, J. L. Slater, M. W. Tate, S. M. Gruner, and A. S. Janoff. 1993. Curvature dependent induction of interdigitated gel phase in DPPC vesicles. *Biochim. Biophys. Acta.* **1146:** 247–257.
41. Komatsu, H., P. T. Guy, and E. S. Rowe. 1993. Effect of unilamellar vesicle size on ethanol-induced interdigitation on dipalmitoylphosphatidylcholine. *Chem. Phys. Lipids.* **65:** 11–21.
42. Zeng, J. W., and P. L. Chong. 1991. Interactions between pressure and ethanol on the formation of interdigitated DPPC liposomes. *Biochemistry.* **30:** 9485–9491.
43. Ohki, K., K. Tamura, and I. Hatta. 1990. Ethanol induces interdigitated gel phase ($L_{\beta I}$) between lamellar gel phase ($L_{\beta'}$) and ripple phase ($P_{\beta'}$) in phosphatidylcholine membranes: a scanning density meter study. *Biochim. Biophys. Acta.* **1028:** 215–222.
44. Boggs, J. M. 1980. Intermolecular hydrogen-bonding between lipids: influence on organization and function of lipids in membranes. *Can. J. Biochem.* **58:** 755–770.
45. Devlin, M. T., and I. W. Levin. 1989. Raman spectroscopic studies of the packing properties of mixed dihexadecyl- and dipalmitoylphosphatidylcholine bilayer dispersions. *Biochemistry.* **28:** 8912–8920.